AIAA 80-1354R

Mixing Mechanism and Structure of an Axisymmetric Turbulent Mixing Layer

M. B. Long* and B. T. Chu†
Yale University, New Haven, Conn.

The mixing mechanism and structure of an axisymmetric mixing layer are studied by a light-scattering technique which provides information on the degree of mixing at 10^4 points in a plane at the same instant. Both qualitative and quantitative results are presented for the range of Reynolds numbers between 10^3 and 10^4. The shear layer leaving the nozzle undergoes a two-stage instability. First, it rolls up into axisymmetric vortices and second, these vortices become unstable to azimuthal disturbances, forming lobe-shaped structures. The enhanced mixing following the second-stage instability is noted and discussed.

I. Introduction

CONSIDERABLE study has been directed in recent years to the near field of a round jet. This surge in interest is prompted in part by a desire to understand (and perhaps to mitigate) the jet noise problem and in part by a growing recognition that the large-scale structure in a turbulent jet is intimately related to the developmental stages of the flow in the mixing layer. Many significant contributions have been made in this connection, and the physical picture which emerges is an interesting one. The shear layer leaving the nozzle, whether it is laminar or turbulent, becomes unstable to form a train of vortex rings, which interact with one another in the course of their motion. The vortex rings in turn become unstable to azimuthal disturbances and ultimately disintegrate into a large number of vortical fragments distributed across the jet. For a detailed description of these changes and references on many earlier contributions and measurements leading to such a picture, see Browand and Laufer[1] and Yule.[2]

The dynamic changes which take place in a jet have a profound influence on the mixing of the jet with its surroundings. It has long been recognized that entrainment of fluids in a turbulent mixing layer is the principal mechanism responsible for enhancing the mixing of two adjacent streams. Direct observation using qualitative flow visualization techniques strongly suggests that the large-scale structure in a turbulent flow is mainly responsible for the entrainment of the nonturbulent fluids into the turbulent stream.[3,4] Results from detailed measurements of the mixing of a hot jet with a cold environment seem to corroborate such a theory.[5-7] A direct and detailed quantitative study of the mixing mechanism is now possible through the use of a technique which allows one to obtain a quantitative two-dimensional mapping of the instantaneous concentration distribution of one of the mixing components in a turbulent flow. Details of this new diagnostic technique are discussed in Ref. 8. The principle of the technique, as it is applied to a study of the mixing of a jet with its surroundings, is outlined below.

Fluid from a 4-mm round nozzle is seeded with uniformly dispersed submicron-sized aerosol particles. By assuming that each unit mass of the nozzle fluid is always "tagged" by approximately the same number of aerosol particles with approximately the same size distribution, the degree of mixing of the "marked" nozzle fluid with the "unmarked" surrounding air will be reflected in a change of aerosol concentration. If a sheet of radiation is allowed to pass through the mixing layer, the distribution of aerosol and, therefore, the nozzle fluid concentration in the sheet at any instant can be monitored and inferred from the distribution of the elastically scattered radiation. The scattered radiation from the sheet is digitized at 10,000 points and stored on computer tape. Subsequently, the record allows one to examine both quantitatively and qualitatively the degree of mixing of the nozzle fluid with the surrounding air. By storing a large number of such records in the computer, statistical information relevant to turbulent mixing can be extracted. The experimental arrangement and apparatus are discussed in Sec. II. The distribution of the mean concentration and the rms concentration fluctuation of the nozzle fluid in the meridian plane are presented in Sec. III. The forms of these distributions are discussed in Sec. IV after examining in some detail the instantaneous concentration distribution of the nozzle fluid in the jet. The dominant mixing mechanisms are discussed in Sec. V. Finally, two examples illustrating how the statistical properties of the constant concentration contours may readily be obtained from the stored data are given in Sec. VI.

II. Experimental Arrangement and Apparatus

All measurements were made on jets from a 4-mm-diam nozzle. The size of the nozzle is the largest which permits efficient light collection and accurate data acquisition, using ordinary commercially available lenses. To minimize the effects of compressibility on turbulent motion, the jet velocity will be restricted to 100 m/s, which is equivalent to a Mach number of less than 0.3 for air under ordinary atmospheric conditions. This places an upper limit on the Reynolds number (based on nozzle diameter) for our facility to 3×10^4, unless special provision is made for pressurizing the system. Here, the jet is exhausted directly into the atmosphere and all measurements are made within the range of a Reynolds number between 10^3 and 10^4.

The nozzle assembly is of a conventional design and is composed of three parts: 1) a conical diffuser with a semivertex angle of 7 deg, 2) a 5.8-cm cylindrical settling chamber equipped with three fine mesh wire screens, and 3) a smooth converging section providing a 211:1 contraction ratio. The freestream turbulent intensity at the nozzle exit is on the order of 0.1%. At a Reynolds number of 4000, the momentum thickness of the boundary layer at the exit is 70 μm and the Reynolds number based on the momentum thickness of the boundary layer is 70. Over the entire range of measurements made, the Reynolds number is well below the critical Reynolds number for which transition to turbulence in

Presented as Paper 80-1354 at the AIAA 13th Fluid and Plasma Dynamics Conference, Snowmass, Colo., July 14-16, 1980; submitted Aug. 18, 1980; revision received March 20, 1981.

*Assistant Professor, Dept. of Engineering and Applied Science.
†Professor, Dept. of Engineering and Applied Science.

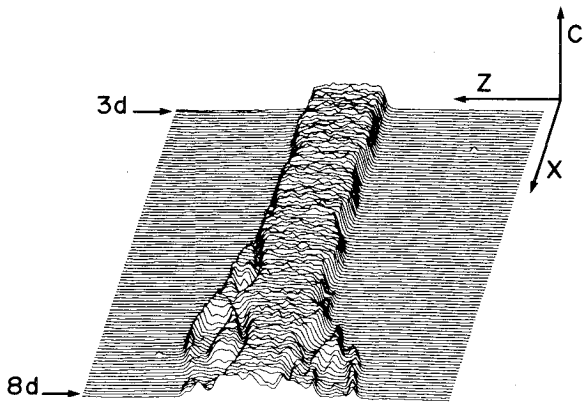

Fig. 1 Instantaneous concentration distribution of the nozzle fluid in a meridian plane at $R = 3240$.

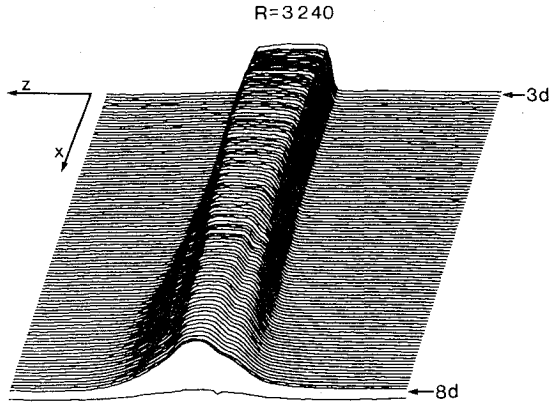

Fig. 2 Mean concentration distribution of the nozzle fluid at $R = 3240$.

the boundary may occur. Therefore, the shear layer leaving the nozzle is laminar.

Submicron-sized sugar aerosols are used to mark the nozzle fluid. Before entering the nozzle assembly, gas from a compressed air source passes through an aerosol generator (Sierra Instruments 7330) where it becomes thoroughly mixed with the aerosols. The homogeneity of the mixture was checked and found to be satisfactory. Since the spatial resolution of the system is ultimately limited by the marker shot noise, the jet is seeded heavily, but not so heavily as to introduce appreciable secondary scattering.

To determine the aerosol concentration (and, therefore, the concentration of the nozzle fluid) in a meridian plane of the jet, radiation from a 2.5 W cw argon ion laser is focused into a thin sheet (0.15 mm thick) passing through the jet axis. Elastically scattered radiation from a 2×2 cm region containing the jet is imaged onto the face of the TV camera (Princeton Applied Research Corp. OMA-2) and is digitized at 10,000 points in a 100×100 array. Each digitized element thus receives scattered radiation from a $0.20 \times 0.20 \times 0.15$ mm^3 volume. In terms of the nozzle diameter, the scattered radiation from the light sheet covering an area of 5×5 nozzle diameters is recorded. In this way, the large-scale structure of turbulence over a span of five jet diameters can be determined. On the other hand, the maximum spatial resolution, expressed in terms of the nozzle diameter d, is only $1/20\ d$, a fact that should be kept in mind when interpreting the results presented below.

To obtain an "instantaneous" concentration distribution, the TV camera is gated on for 10 μs. While the scattered radiation from 10^4 volume elements is recorded almost "instantaneously," conversion of each analog signal to a digital signal requires approximately 80 μs, so that a total of 80×10^4 μs will have elapsed before the system is ready for recording another "picture." Successively digitized images are, therefore, essentially independent events and statistical quantities presented here are obtained by averaging over 1000 independent realizations of the same flow. A schematic diagram of the experimental arrangement, as well as other experimental details, may be found in Ref. 8.

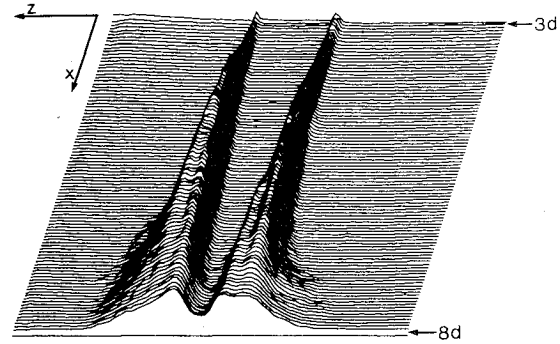

Fig. 3 The rms concentration fluctuations at $R = 3240$.

III. Mean and rms Concentration

Figure 1 gives an example of the instantaneous nozzle fluid distribution in a meridian plane of a jet. In the figure, the x axis points in the direction of the flow, the xz plane coincides with a meridian plane, and the concentration of the nozzle fluid $C(x,z)$ is displayed as the height above the xz plane. The Reynolds number R is 3240 and the markings in the figure, 3 d and 8 d, signify locations 3 and 8 diameters downstream from the nozzle exit. The figure gives a graphic representation of the digitized concentration at 10,000 points. The mean concentration of the nozzle fluid in a meridian plane is obtained by averaging these concentrations over 1000 realizations. This is shown in Fig. 2. The mean concentration has nearly a top-hat distribution at $x = 3\ d$, while at 8 d it approaches a bell-shaped distribution. It is noteworthy that the mean concentration profile develops a "shoulder" between 4 and 5 d, which persists until 8 d. Thus, in this range, the concentration profile in the mixing layer has three inflection points, in sharp contrast to the familiar distribution of the mean velocity profile which has been extensively explored and documented.[9] The same phenomenon is observed at higher Reynolds numbers.

The existence of triple inflection points in the concentration profile can be detected in some of the published results of Brown and Roshko.[4] It was probably noticed by other investigators, but it was Fiedler[5] who first called attention to this interesting feature in a two-dimensional mixing layer. Fiedler also established the similarity property of the profile and suggested that it is the result of a mixed transport mechanism in which vortex motion plays a major part.[5,6] Similar distributions in an axially symmetric turbulent mixing layer were found by Sreenivasan et al.[7]

The rms distribution of concentration fluctuations in the meridian plane for the same flow is shown in Fig. 3. A "depression" in the rms profile begins to emerge somewhere between 4 and 5 d, at about the same location where the shoulder first appears in the mean concentration profile. The depression at first deepens as one proceeds downstream, but ultimately disappears at about the same location where the shoulder in the mean concentration profile vanishes (i.e., a short distance beyond 8 d). There is little doubt that the depression in the rms profile and the shoulder in the mean concentration profile are closely related and could be ascribed to the same cause. The existence of the two maxima and one minimum in the rms profile for the two-dimensional mixing layer was also pointed out by Fiedler.[5]

Some care must be exercised in interpreting the concentration distribution obtained by nondiffusive markers such as our aerosol particles in regions where the relevant

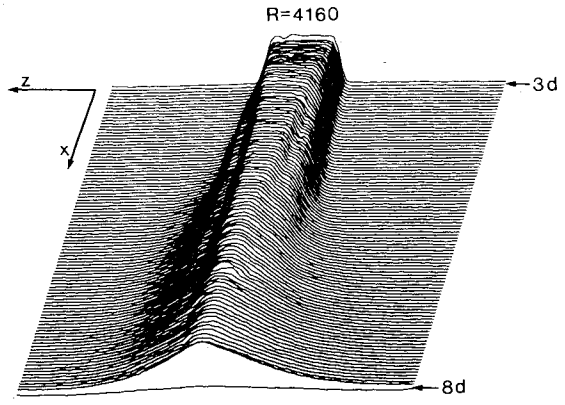

Fig. 4 Mean concentration distribution in a meridian plane at $R = 4160$.

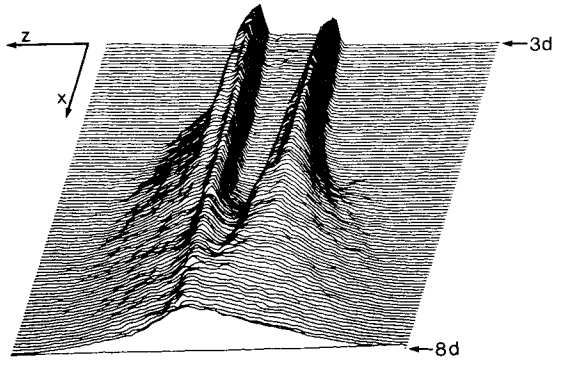

Fig. 5 The rms concentration fluctuations at $R = 4160$.

macroscale is small and the mixing process is dominated by molecular transport. For example, the laminar shear layer near the nozzle exit has a thickness on the order of that of the laminar boundary layer leaving the nozzle, e.g., 70 μm at $R = 4000$. Diffusion of the nozzle fluid in this thin region is undetectable by our system. Not until the shear layer becomes unstable and oscillates with an amplitude exceeding the smallest resolvable scale (i.e., 0.20 mm or 1/20 of the nozzle diameter) does one expect to see a broadening of the mixing layer marked by our nondiffusive particles.

As the Reynolds number is increased, all the length scales characterizing the various changes decrease. Thus, the mean concentration profile departs from the top-hat distribution much closer to the nozzle exit. The shoulder in the mean concentration and the depression in the rms fluctuation occur much sooner. This is clear from Figs. 4 and 5 where the average concentration and rms distribution in the same region (i.e., between 3 and 8 d) at a slightly higher Reynolds number of 4160 are shown. Note the "billowing" of the rms profile beyond 4.5 d. The same effect can also be detected (though not as clearly) in the average concentration distribution (Fig. 4). It signifies the rapid increase of mixing which follows. The high sensitivity with which the locations of the various salient features of the mean concentration and rms profiles vary with a change in Reynolds number from 3240 to 4160 signifies that the growth rate of the finite amplitude unstable mode is strongly dependent on the Reynolds number in this range.

The concentration profile can be expected to be similar in the region where the mixing layer is thick, compared to the thickness of the original shear layer, but thin in comparison with the radius of the jet. This region, if it exists, is short for flows with higher Reynolds numbers. To locate such a region, we shall display the average concentration shown in Fig. 2 ($R = 3240$) in a different form, as shown in Fig. 6. In actuality, the figure is a superposition of four shaded areas, representing regions where the concentration of the nozzle fluid is greater than or equal to 20, 40, 60, and 80% of the

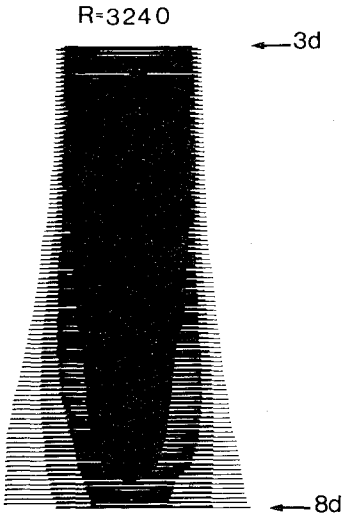

Fig. 6 Boundaries of equally shaded regions are contours of equal mean concentration of the nozzle fluid ($R = 3240$).

initial (maximum) concentration. For the sake of clarity, these shaded regions are slightly staggered in Fig. 6. The net effect is that regions with heavy shading represent those where there is a higher nozzle fluid concentration. The boundaries of each of the uniformly shaded regions, of course, represent contours of constant concentration.

To establish the similarity in the mean concentration profile and determine the rate of spread of the mixing layer in this region, it is necessary to locate those parts of the constant concentration contours which are approximately straight lines that converge to a single point. For a more accurate determination of the rate of spread, the scale in the z direction (i.e., across the jet) is amplified in comparison to that used in the x direction. The rate of spread, expressed as the increase of the width between the 20 and 80% lines per unit axial distance, is found to be 0.16.

In the next section, we shall attempt to discover the "reasons" for the above observations. This should be possible because the spatial structure of the mean concentration distribution is obtained by averaging over a large number of instantaneous concentration distributions. The mean rms concentration distributions must be a reflection of some of the common properties of the instantaneous distributions. It is in this connection that the technique we use is especially valuable for interpreting the statistically averaged quantities.

IV. Instantaneous Concentration Distributions

The instantaneous concentration distribution of the nozzle fluid in a meridian plane (Fig. 1) contains a tremendous amount of detail. Since there are substantial variations in the concentration distributions in different realizations of the same flow, it presents a difficult task to extract the common features shared by these distributions by examining a large number of realizations. A more useful approach is to sacrifice some detail and display the instantaneous concentrations of the nozzle fluid in regions where the concentration is greater than or equal to 20, 40, 60, and 80% of the initial concentration of the nozzle fluid, just as the mean concentration is displayed in Fig. 6.

Figures 7a and 7b give two superficially very different concentration distributions of the same flow ($R = 3240$). They differ in that, while a more or less regular train of lobed structures appears in Fig. 7b, mixing in Fig. 7a is decidedly irregular, asymmetric, and "violent." On closer examination, however, one can detect many common features shared not only by the two distributions shown but by all the others as well. Both figures suggest that, as the flow leaves the nozzle, mixing of the nozzle fluid with the surrounding air is at first

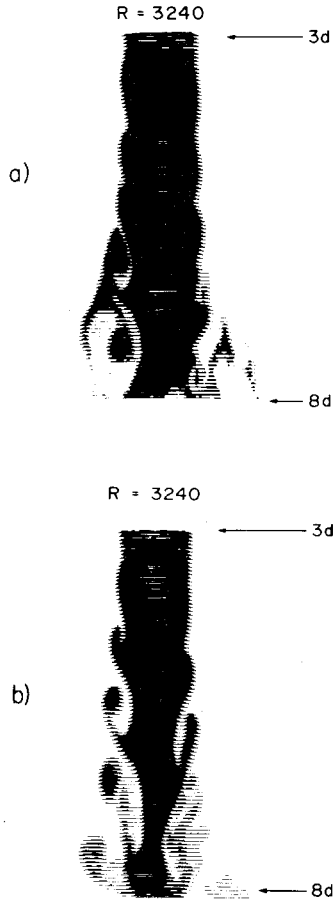

Fig. 7 Contours of constant instantaneous nozzle fluid concentration in a meridian plane for two realizations at $R = 3240$. Different shaded regions correspond to those where the concentration is greater than or equal to 20, 40, 60, and 80% of the maximum concentration.

confined to a thin layer which assumes a somewhat undulating shape. This is in agreement with the dynamic picture that the shear layer leaving the nozzle is unstable. The lobed structure in Fig. 7b is then the cross section of the vortex rings. The fine internal spiral structure of these rings cannot be detected because the limited spatial resolution of our present system does not permit us to resolve any structures whose width is less than one-tenth of the nozzle diameter. By the same token, the absence of any distinctive lobed structure in Fig. 7a prior to the onset of the violent mixing may well be explained on the same basis. From this viewpoint, the violent mixing may be identified with the disintegration of vortex rings resulting from azimuthal instability. This view is supported by the fact that the lobed structure in Fig. 7b does indeed break down into a state of violent mixing near 8 d, as indicated by the widespread and asymmetric distribution of nozzle fluid there. Thus, Figs. 7a and 7b differ only in the exact location where the violent mixing occurs. The same conclusions are reached by examining other realizations in the same flow.

Essentially the same sequence of events is observed for flow at other Reynolds numbers except that as the Reynolds number increases, the shear layer rolls into vortex rings much closer to the nozzle exit, and these vortex rings disintegrate much sooner so that a long train of lobed structures [as in Fig. 7b] is seldom found prior to the onset of the violent mixing.

To test the concept that the violent mixing is associated with the disintegration of vortex rings, the distribution of nozzle fluid is examined in a plane perpendicular to the axis of the jet at a location where the violent mixing is sometimes observed. Figures 8a and 8b show two realizations of the same flow.

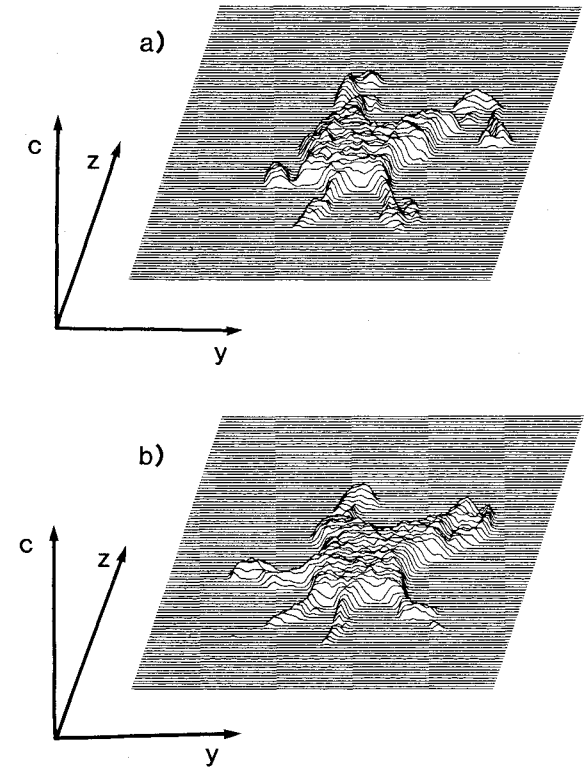

Fig. 8 Nozzle fluid distributions in a plane perpendicular to the axes of the jet.

Fig. 9 Instantaneous nozzle fluid concentration distribution in a meridian plane at $R = 4160$.

Both distributions have a starlike structure, one possessing five lobes and the other six, suggesting that they are the result of the azimuthal instability of a vortex ring. According to Widnall and Sullivan,[10] a vortex ring in an ideal flow is almost always unstable and the number of waves around the perimeter depends on the core size of the vortex ring.

Figure 9 provides some additional insight on the distribution of the nozzle fluid in the violent mixing region. The Reynolds number is 4160 and the distribution in a meridian plane is shown. The onset of violent mixing occurs at about 6 d. The enhancement in mixing beyond this point is evident. Here, the lightly shaded (low concentration) regions penetrate deep into the heavily shaded (high concentration) regions, and "pockets" of unshaded regions are trapped between the shaded regions. Moreover, patches of nozzle fluid find their way to the outer rim of the jet boundary, as is evident from the narrow strips and small patches of heavily

shaded "islands" in the lightly shaded regions. The picture is interesting because it catches one of the ring vortices penetrating into the violent mixing region before it disintegrates like the other vortices preceding it.

We are now in a position to give an explanation of the mean and rms concentration profiles observed. First, the onset of the violent mixing (Figs. 7 and 9) may obviously be described as a billowing of the instantaneous profile. Consequently, the more "gentle" billowing of the mean and rms concentration profiles may be ascribed to the disintegration of vortex rings. The billowing is more gentle here because the vortex disintegration does not occur at a fixed location.

The train of vortex rings prior to their disintegration causes a redistribution of the nozzle fluid as shown in Fig. 7b. Two features of this distribution are noteworthy. The vortex structure appears to grow linearly from an apex as it would if there is no relevant length scale controlling its evolution.

Second, the redistribution of the nozzle fluid is such that, unlike ordinary diffusion where the concentration decreases radially outward, the average concentration along any radial line through the apex first decreases, then increases, and finally decreases again as this line is rotated outward about the apex (i.e., rotated from the high-speed side to the low-speed side of the mixing layer). When a large number of such vortex structures are averaged, the net effect is to cause a transport of the nozzle fluid to the low-speed side of the mixing layer, augmenting the concentration there at the expense of the nozzle fluid in the center of the mixing layer. Thus, vortical transport is responsible for producing a shoulder on the mean concentration profile, as well as for the development of two maxima and one minimum in the rms profile, since the latter is a measure of the deviation of the fluctuations from the mean.

V. Entrainment and the Mixing Mechanisms

One distinctive feature which shows up especially clearly in many realizations of the flow at lower Reynolds numbers can be seen in Fig. 7b. Each of the vortices is attached to the densely shaded core region of the main jet by a long "umbilical cord." Of course, they should not be interpreted as cords; rather, they are thin annular layers of nozzle fluid which connect the vortex rings with the fluid in the core region of the jet. A large amount of ambient air is trapped by this engulfing surface and, in due course, is mixed and "digested" by the vortical fluid in the mixing layer.

The origin of such engulfing layers can also be easily understood. The shear layer rolls into vortex rings, which at first lie close to the surface of the main core of nozzle fluid. Since the vortex rings are, in fact, convoluted shear layers, they are connected to the main jet through a thin layer of nozzle fluid. As a vortex ring gathers strength as a result of the shear-layer instability, it continues to pump the core fluid into the layer and the ambient air into the fold. This produces a radial pressure field which depresses and "squeezes" the main core of the jet, while forcing the center of the vortex to drift outward into the slower moving medium around the jet. The vortex thus "falls behind" the main jet, resulting in a stretching out of the umbilical layer into a long, thin sheet of nozzle fluid, trapping an annular wedge of the ambient air between the engulfing sheet and the core region of the jet. Such a structure is very evident in Fig. 7b and can also be recognized in Fig. 7a. This process continues even after the vortex ring has entered the region of violent mixing and is surrounded by the debris produced by the disintegration of earlier vortex rings. This mechanism of mixing, which may be described as the "vortex mixing mechanism," is responsible for the shoulder in the average concentration profile. This mixing mechanism remains operative even if the flow is not turbulent. Indeed, in many instances, the flow is not turbulent prior to the vortex breakdown.[2,11]

A second mixing mechanism operative in the flow is reflected in the onset of violent mixing in Figs. 7a and 9. As we have noted, the azimuthal instability of a vortex ring results in a disintegration of the ring. In this process, the vortical fluid from the core of the vortex ring is projected outward as shown in Fig. 8 and is mixed with fragments of vortical fluid left behind by the breakdown of earlier vortex rings. The net effect is well illustrated in Fig. 9, where one vortex ring manages to remain intact as it penetrates into the region of violent mixing, while the remnant of the preceding one can be vaguely identified. The motion generated by the distributed vorticity is definitely turbulent in this region, although it is not known for certain if the small-scale fluctuations arise from the fragmented core of a vortex ring which has become turbulent or from the action of the radial jets produced in the ejection process (Fig. 8).

The long strips of more densely shaded areas in the region of violent mixing in Fig. 9 betray the origin of the fluid occupying them. The relative forward motion of different parts of the jet in this region is responsible for their elongated shape. The small-scale fluctuations due to the distributed vortical material are responsible for the general smearing of concentration in the region.

VI. Some Statistical Properties of Constant Concentration Contours

In this section, we shall present some preliminary results on two average properties of constant concentration contours. Such contours are of importance in studying turbulent mixing and in certain combustion problems. Thus, the so-called viscous superlayers which form the boundaries between the fluid in the mixing layer and that outside it can be determined by introducing an indicator function which is equal to unity at a point where the nozzle fluid concentration is between C_n and $C_{max} - C_n$ and is zero otherwise. Here C_{max} denotes the maximum concentration and C_n characterizes the noise level in the concentration signal. Likewise, in a turbulent diffusion flame, combustion occurs at that constant concentration surface where the ratio of the reactants is in stoichiometric proportion.

To determine the statistical properties of a constant concentration contour, the first step is to trace out such a curve for each of the realizations obtained in an experiment. Thus, the contour on which the nozzle fluid has a concentration equal to $0.4C_{max}$ can be obtained for each realization by introducing the indicator function

$$I(x,z) = \begin{cases} 1 & \text{for } C/C_{max} > 0.4 \\ 0 & \text{otherwise} \end{cases}$$

Fig. 10 Regions where the instantaneous concentration is greater than or equal to 40% of the maximum nozzle fluid concentration are shaded. The boundaries of these regions are contours where the concentration of the nozzle fluid is $0.40C_{max}$ at $R = 4160$.

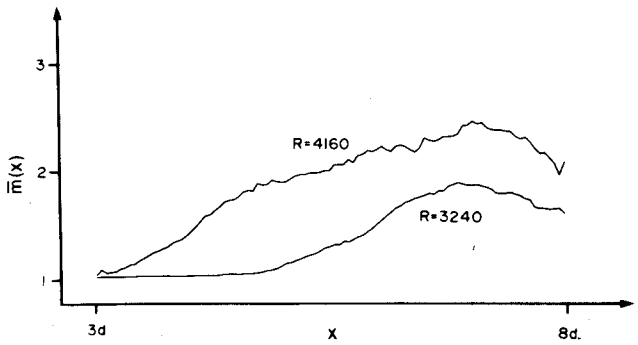

Fig. 11 Average number of intersections of the constant concentration contour $C=0.5C_{max}$ with the line $x=$ const.

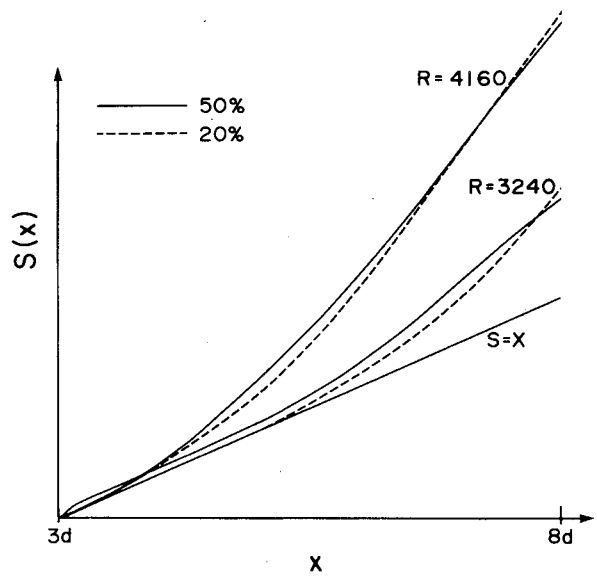

Fig. 12 Arc lengths of the $0.20C_{max}$ and $0.50C_{max}$ contours at $R=3240$ and 4160.

This function is shown in Fig. 10 for one such realization at $R=4160$. In the figure, $I(x,z)$ has the value of unity in the shaded regions and the value zero in the unshaded regions. The boundary of the shaded region is, of course, the required constant concentration contour.

A salient feature of such contours is that they generally intersect lines parallel to the z axis at more than one point. In other words, if such a contour is described by the function $z=z(x)$, then $z(x)$ is a multivalued function of x. A discussion of the general statistical description of a multivalued random function, especially with a view of its applications to problems in turbulence, has been given by Lumley.[12] The complete statistical description of a constant concentration contour can, in principle, be determined from a sufficiently large collection of instantaneous concentration distributions. Unfortunately, the size of such a collection proves to be impractically large. Some of the simpler statistical properties can be computed directly, however, without recourse to a complete statistical description. For example, Fig. 11 gives the average number of intersections, $\bar{m}(x)$, of a constant concentration contour with a line $x=$const. In Fig. 12, the arc length of a constant concentration contour, $S(x)$, measured from an arbitrarily chosen point x_0, is shown. To be sure, where x_0 is chosen is inconsequential because it is the derivative of $S(x)$ which is of interest, as the derivative is a measure of the increase in the arc length per unit axial displacement. Four curves are displayed in the figure, representing the 20 and 50% contours at 3240 and 4160, respectively. The straight line $S=x$ is included to indicate how the Sx curve should appear in the ideal case of a straight-line contour which is parallel to the x axis. Two interesting conclusions may be deduced: 1) the arc lengths for the 20 and 50% contours differ from one another only slightly; 2) the arc lengths of these contours increase rapidly as the Reynolds number is increased. A systematic study of the statistical properties of the constant concentration contour is in progress.

VII. Conclusions

The scattering technique employed has provided not only quantitative data but also qualitative information useful in interpreting the data. Thus, it establishes the unique features of the mean concentration and the rms distributions in an axial symmetric mixing layer, while allowing one to gain a deeper insight into the underlying causes of such distributions.

Two major mixing mechanisms are identified: 1) the vortex mixing mechanism, which is responsible for the peculiar distribution of average concentration and rms fluctuations, and 2) the jet mixing mechanism, resulting from the breakdown of vortex rings and leading to outward projections of the vortical fluid from the center part of the flow. Finally, the method also provides a means for determining several average properties of the constant concentration contours.

Acknowledgments

We are indebted to Prof. Richard K. Chang who provided the initial inspiration leading to this work, to Prof. K. R. Sreenivasan for many helpful discussions and suggestions, and to Miss Carla Escoda for assistance with some of the experiments. We also gratefully acknowledge the Office of Naval Research, Project SQUID, for partial support of this work under Contract No. N00014-79-C-0254.

References

[1] Browand, F. K. and Laufer, J., "The Role of Large Scale Structures in the Initial Development of Circular Jets," Proceedings of the 4th Biennial Symposium, *Turbulence in Liquids,* University of Missouri-Rolla, Science Press, Princeton, N. J., 1975, pp. 333-344.

[2] Yule, A. J., "Large-Scale Structure in the Mixing Layer of a Round Jet," *Journal of Fluid Mechanics,* Vol. 89, Pt. 3, 1978, pp. 413-432.

[3] Townsend, A. A., *The Structure of Turbulent Shear Flow,* Cambridge Press, Cambridge, England, 1956.

[4] Brown, G. L. and Roshko, A., "On Density Effects and Large Structure in Turbulent Mixing Layers," *Journal of Fluid Mechanics,* Vol. 64, Pt. 4, 1974, pp. 775-816.

[5] Fiedler, H. E., "Transport of Heat across a Plane Turbulent Mixing Layer," *Advanced Geophysics,* Vol. 18A, 1974, pp. 93-109.

[6] Fiedler, H. E., "On Turbulence Structure and Mixing Mechanism in Free Turbulent Shear Flows," in *Turbulent Mixing in Non-Reactive and Reactive Flows,* edited by S. N. B. Murthy, Plenum Press, New York, 1975, pp. 381-407.

[7] Sreenivasan, K. R., Antonia, R. A., and Stephenson, S. E., "Conditional Measurements in a Heated Axisymmetric Turbulent Mixing Layer," *AIAA Journal,* Vol. 16, No. 1978, pp. 869-870.

[8] Long, M. B., Chu, B. T., and Chang, R. K., "Instantaneous Two-Dimensional Gas Concentration Measurements by Light Scattering," *AIAA Journal,* Vol. 19, Sept. 1981, pp. 1151-1157.

[9] Bradshaw, P., Ferriss, D. H., and Johnson, R. F., "Turbulence in the Noise-Producing Region of a Circular Jet," *Journal of Fluid Mechanics,* Vol. 19, 1964, pp. 591-624.

[10] Widnall, S. E. and Sullivan, J. P., "On the Stability of Vortex Rings," *Proceedings of the Royal Society of London, Series A,* Vol. 332, 1973, pp. 335-353..

[11] Chandrsuda, C., Mehta, R. D., Weir, A. D., and Bradshaw, P., "Effect of Free-Stream Turbulence on Large Structure in Turbulent Mixing Layers," *Journal of Fluid Mechanics,* Vol. 85, Pt. 4, 1978, pp. 693-704.

[12] Lumley, J. L., *Stochastic Tools in Turbulence,* Academic Press, New York, 1970.